(2)

AFWAL-TR-89-3020

A NUMERICAL STUDY OF THREE-DIMENSIONAL SEPARATED FLOWS AROUND A SWEPTBACK BLUNT FIN

Universal Energy Systems, Inc.
4401 Dayton-Xenia Road
Dayton, Ohio 45432

2 February 1989

Final Report for Period October 1987 - July 1988

Approved for Public Release; Distribution is Unlimited

FLIGHT DYNAMICS LABORATORY
WRIGHT RESEARCH AND DEVELOPMENT CENTER
AIR FORCE SYSTEMS COMMAND
WRIGHT-PATTERSON AFB, OHIO 45433-6523

NOTICE

When Government drawings, specifications, or other data are used for any purpose other than in connection with a definitely Government-related procurement, the United States Government incurs no responsibility or any obligation whatsoever. The fact that the Government may have formulated or in any way supplied the said drawings, specifications or other data, is not to be regarded by implication, otherwise in any manner construed, as licensing the holder, or any other person or corporation; or as conveying any rights or permission to manufacture, use, or sell any patented invention that may in any way be related thereto.

This report has been reviewed by the Office of Public Affairs (ASD/PA) and is releasable to the National Technical Information Service (NTIS). At NTIS, it will be available to the general public, including foreign nations.

This technical report has been reviewed and is approved for publication.

Joseph J. S. Shang

JOSEPH J. S. SHANG, Tech Mgr
Computational Aero Group
Aerodynamics and Airframe Br

Dennis Sedlock

DENNIS SEDLOCK, Acting Chief
Aerodynamics and Airframe Br
Aeromechanics Division

FOR THE COMMANDER

Alfred C. Draper

ALFRED C. DRAPER
Acting Chief, Aeromechanics Division
Flight Dynamics Laboratory

If your address has changed, if you wish to be removed from our mailing list, or if the addressee is no longer employed by your organization please notify AFWAL/FIMM, Wright-Patterson AFB, OH 45433-6553 to help us maintain a current mailing list.

Copies of this report should not be returned unless return is required by security considerations, contractual obligations, or notice on a specific document.

UNCLASSIFIED
SECURITY CLASSIFICATION OF THIS PAGE

REPORT DOCUMENTATION PAGE

Form Approved OMB No. 0704-0188

1a. REPORT SECURITY CLASSIFICATION
UNCLASSIFIED

1b. RESTRICTIVE MARKINGS

2a. SECURITY CLASSIFICATION AUTHORITY

2b. DECLASSIFICATION / DOWNGRADING SCHEDULE

3. DISTRIBUTION / AVAILABILITY OF REPORT
Approved for public release; distribution is unlimited.

4. PERFORMING ORGANIZATION REPORT NUMBER(S)

5. MONITORING ORGANIZATION REPORT NUMBER(S)
AFWAL-TR-89-3020

6a. NAME OF PERFORMING ORGANIZATION
Universal Energy Systems, Inc.

6b. OFFICE SYMBOL *(If applicable)*

7a. NAME OF MONITORING ORGANIZATION
Flight Dynamics Laboratory (AFWAL/FIMM)
Air Force Wright Aeronautical Laboratories

6c. ADDRESS *(City, State, and ZIP Code)*
4401 Dayton-Xenia Road
Dayton OH 45432

7b. ADDRESS *(City, State, and ZIP Code)*
Wright-Patterson AFB OH 45433-6553

8a. NAME OF FUNDING / SPONSORING ORGANIZATION

8b. OFFICE SYMBOL *(If applicable)*

9. PROCUREMENT INSTRUMENT IDENTIFICATION NUMBER
F33615-86-C-3800

8c. ADDRESS *(City, State, and ZIP Code)*

10. SOURCE OF FUNDING NUMBERS

PROGRAM ELEMENT NO	PROJECT NO.	TASK NO	WORK UNIT ACCESSION NO
61102F	2307	N6	11

11. TITLE *(Include Security Classification)*
A Numerical Study of Three-Dimensional Separated Flows Around a Sweptback Blunt Fin

12. PERSONAL AUTHOR(S)
D. L. McMaster and Dr J. S. Shang

13a. TYPE OF REPORT	13b. TIME COVERED	14. DATE OF REPORT (Year, Month, Day)	15. PAGE COUNT
Final Report	FROM Oct 87 TO Jul 88	2 Feb 89	34

16. SUPPLEMENTARY NOTATION

17. COSATI CODES

FIELD	GROUP	SUB-GROUP
01	01	
01	03	

18. SUBJECT TERMS *(Continue on reverse if necessary and identify by block number)*

19. ABSTRACT *(Continue on reverse if necessary and identify by block number)*

A series of numerical simulations was carried out for supersonic flow past a blunt fin mounted on a flat plate with progressively increasing leading edge sweepback. The numerical result for zero degree sweep (vertical fin) was first validated with a known numerical solution and experimental data at Mach 2.95 and unit Reynolds number of 64 million per meter. The upstream condition of the interacting region was characterized by a fully developed turbulent boundary layer with a thickness identical to that of the fin diameter. The upstream and spanwise influence of the fin decreased significantly with increasing sweepback. Under the given flow conditions, the bifurcation of the phase portrait of the surface shear-stress vector was observed between the sweepback angles of 60 to 80 degrees. ([illegible])

20. DISTRIBUTION / AVAILABILITY OF ABSTRACT
☒ UNCLASSIFIED/UNLIMITED ☐ SAME AS RPT ☐ DTIC USERS

21. ABSTRACT SECURITY CLASSIFICATION
UNCLASSIFIED

22a. NAME OF RESPONSIBLE INDIVIDUAL
Dr Joseph J. S. Shang

22b. TELEPHONE *(Include Area Code)*
(513) 255-7127

22c. OFFICE SYMBOL
AFWAL/FIMM

FOREWORD

A series of numerical simulations was carried out for supersonic flow past a blunt fin mounted on a flat plate with progressively increasing leading edge sweepback. The numerical result for zero degree sweep (vertical fin) was first validated with a known numerical solution and experimental data at Mach 2.95 and unit Reynolds number of 64 million per meter. The upstream condition of the interacting region was characterized by a fully developed turbulent boundary layer with a thickness identical to that of the fin diameter. The upstream and spanwise influence of the fin decreased significantly with increasing sweepback. Under the given flow conditions, the bifurcation of the phase portrait of the surface shear-stress vector was observed between the sweepback angles of 60 to 68 degrees.

LIST OF CONTENTS

LIST OF FIGURES

LIST OF SYMBOLS

D	leading edge diameter of the blunt fin
e	internal energy
F,G,H	flux vectors, equation (1)
k	heat conductivity
M	Mach number
p	pressure
Re	unit Reynolds number
t	time
T	temperature
$\bar{U}$	dependent variable vectors, equation (1)
u,v,w	velocity components in the Cartesian frame
x,y,z	coordinates in the Cartesian frame
$y+$	law of the wall coordinate
Λ	leading edge sweepback angle of fin
η	scaling length
ρ	density
$\tilde{\tau}$	stress tensor

Subscript

∞	denotes conditions evaluated at the free stream
w	denotes conditions at the wall

ACKNOWLEDGEMENT

The computing resources provided by the NAS Systems Division, NASA Ames Research Center are gratefully acknowledged.

SECTION I

INTRODUCTION

Maneuverable supersonic and hypersonic flight vehicles require a variety of control surfaces that generate complex flow patterns.[1] One common example of such a control surface is a blunt fin, which at locally supersonic flow conditions can induce a shock/boundary layer interaction associated with flow separation.[2-7] The baseline case for the blunt fin control surface is the blunt fin on a flat plate at zero angle of attack to the freestream, as shown in Figure 1. Although this configuration has been previously investigated both experimentally and numerically, much remains unknown about the flow field, especially at non-zero sweepback angles. The objective of the present research is to establish computational evidence describing the effect of the sweepback angle, Λ, on the number and strength of the upstream vortical structures associated with diverting flow past the fin. For the case of the vertical fin (Λ=0), Hung et al[6,7] predicted the nature of the flow field structure using numerical studies based on previous experiments.[4,5] Their results showed the formation of a pair of horseshoe vortices upstream of the fin, with the primary vortex diverting entrained freestream fluid past the

fin. Other numerical work by Shang and Scherr,[8] however, indicated that a highly swept fin on a complex configuration had no associated upstream horseshoe vortex to divert the fluid. Earlier experimental evidence[2,3] also indicated that sweepback had an effect in reducing the upstream influence of a fin, although no firm conclusions were made about the existence or strength of vortical structures.

The above results indicate that the flow structure should undergo a bifurcation at a sweepback angle sufficiently high that the horseshoe vortex upstream of the fin leading edge ceases to exist. At this juncture, an associated change must take place in the topological phase portrait on the surface of the flat plate.[9] In addition, the decrease in upstream influence associated with increased fin sweepback should also coincide with a less pronounced spanwise propagation of flow disturbances. This information is important, since vortical structures can cause significant variations in pressure and rate of heat transfer on neighboring surfaces as well as on the blunt fin itself, thus altering control effectiveness in the entire region near the fin.

A two step procedure was followed to determine the effect of fin sweepback on the upstream topological structure and spanwise propagation of flow disturbances. Results were first

calculated echoing the vertical blunt fin flow conditions used by previous numerical and experimental investigators.[4-7] The stagnation temperature and pressure were 260 K and 6.8×10^5 Nm^{-2}, respectively. The freestream Mach number was 2.95, yielding a unit Reynolds number of 64 million per meter. The boundary layer was fully turbulent with a thickness of 1.27 cm at the fin leading edge. The fin leading edge diameter was also 1.27 cm. The computations were accomplished using a three-dimensional finite difference explicit code based on MacCormack's 1969 predictor-corrector algorithm.[10] Once the code was verified for the vertical fin, it was utilized under the same upstream flow conditions for increasing fin sweep to assess the formation and strength of the vortical structures as a function of the sweep angle. This procedure was continued until the bifurcation point, reflected by a change in the phase portrait of the surface shear stress vector, was reached.

SECTION II

ANALYSIS

1. TOPOLOGICAL BIFURCATION

Any three-dimensional flow field must satisfy topological rules which arise from the requirement of flow continuity. A separated flow can be characterized by the number of node and saddle points on a given plane cutting the three dimensional flow field; traditionally, the flow adjacent to a surface is represented by the skin-friction line pattern formed by experimental oil streaks. The status of the surface shear flow pattern is termed the phase portrait of the surface shear stress vector (path-preserving mapping). If the character of the phase portrait changes due to a change in some external flow parameter, the phase portrait is said to undergo bifurcation.[9] The flow past a vertical blunt fin is characterized by a surface oil pattern on the flat plate that includes a convergence line (indicating that flow leaves the surface to roll up into the horseshoe vortex) and a divergence line (indicating reattachment) upstream of the fin leading edge. This pattern is seen in the numerically simulated oil patterns of Figure 2, which was taken from Reference 7.

In contrast to the pattern seen for the vertical fin, Figure 3 shows the surface shear pattern near a highly swept fin on a complex body, as computed in Reference 8. Here, the absence of a set of convergence and divergence lines upstream

of the fin indicates fully attached, vortex-free flow. Thus given a flow represented by the surface shear portrait shown in Figure 2, if one were to increase the fin sweepback angle, at some sufficiently large sweepback angle the surface shear pattern should bifurcate. The surface shear portrait would then be similar to that in Figure 3, characterized by the absence of distinct convergence and divergence lines upstream of the fin.

2. GOVERNING EQUATIONS

The flow under consideration can be described by the fully three dimensional, mass-averaged Navier-Stokes equations with an algebraic turbulence model:

$$\frac{\partial U}{\partial t} + \frac{\partial F}{\partial x} + \frac{\partial H}{\partial y} + \frac{\partial G}{\partial z} = 0 \qquad (1),$$

where

$$U = \begin{bmatrix} \rho \\ \rho u \\ \rho v \\ \rho w \\ \rho e \end{bmatrix}$$

$$F = \begin{bmatrix} \rho u \\ \rho u^2 + \tau_{xx} \\ \rho uv + \tau_{xy} \\ \rho uw + \tau_{xz} \\ (\rho e + \tau_{xx})u + \tau_{xy}v + \tau_{zx}w - k\frac{\partial T}{\partial x} \end{bmatrix}$$

$$G = \begin{bmatrix} \rho v \\ \rho uv + \tau_{xy} \\ \rho v^2 + \tau_{yy} \\ \rho vw + \tau_{yz} \\ (\rho e + \tau_{yy})v + \tau_{yx}u + \tau_{yz}w - k\frac{\partial T}{\partial y} \end{bmatrix}$$

$$H = \begin{bmatrix} \rho w \\ \rho uw + \tau_{xz} \\ \rho vw + \tau_{yz} \\ \rho w^2 + \tau_{zz} \\ (\rho e + \tau_{zz})w + \tau_{xz}u + \tau_{yz}v - k\frac{\partial T}{\partial z} \end{bmatrix}$$

The assumption is made that the mass-averaged equations represent the ensemble average of the flow, even though the flow is unsteady due to shock oscillation.[4,5] The frequency of the shock oscillation is in the kHz range, and the assumption is supported by the referenced experimental findings which exhibit no unsteadiness in the measurements of the mean flow properties.

3. NUMERICAL PROCEDURES

The numerical scheme for the present study is MacCormack's 1969 predictor-corrector method, which has been shown to yield accurate results for high-Reynolds number supersonic flows.

The computational grids were algebraically generated, and were dimensioned 40 x 32 x 32 in the streamwise, spanwise, and vertical directions, respectively. The grid structure for the vertical fin ($\Lambda=0°$) is very similar to that used in References 6 and 7. However, the minimum grid spacing of .00433D used in the referenced numerical work was found to be too coarse for the present purpose, because it yields a value of y+ at the wall of ~30. While this resolution may be sufficient to capture the major structures of the flow past the vertical fin, since those structures are predominately inviscid, the ability to predict the upstream flow field near the fin-flat plate juncture for configurations of high sweepback was seriously degraded by inadequate resolution of the viscous region. Therefore a minimum grid spacing of .001D was used at the flat plate surface for all the grids that were dimensioned 40 x 32 x 32. This resulted in a y+ at the wall of ~10. In the direction normal to the fin, however, the minimum spacing at the fin surface was kept at .004D. This created a less severe stretching in the normal direction, which maintained sufficient resolution upstream of the fin leading edge near the

experimentally determined location of the convergence of the surface shear-stress lines. Figure 4a is an elevated view of the grid used to compute the flow past the vertical fin. The sweptback grids were generated using the grid for the vertical fin by moving each horizontal plane rearward an appropriate amount according to the sweepback angle. Figure 4b shows the elevated view of the grid for the 60° swept fin. The severity of the stretching of individual cells for this grid can be seen in Figure 4c, which is a closeup of the grid cells near the fin-flat plate junction on the plane of symmetry.

The turbulence model was the Baldwin-Lomax eddy viscosity model, with a modified scaling length designed to take into account the presence of two walls. In this formulation, the scaling length is

$$\eta = \frac{2yz}{y + z + (y^2 + z^2)^{0.5}} \qquad (2),$$

where z and y are the normal distances from the two walls. The general formulation of the eddy viscosity near two walls was considered in detail in previous references[7,11,12] and is not explained here.

The boundary conditions were essentially the same as those used in Reference 7. The upstream boundary condition was prescribed as the fully turbulent flat plate boundary layer of thickness 1.27 cm, matching the fin leading edge diameter. This was obtained by computing the flow on a flat plate until convergence, and using the station with the appropriate boundary layer thickness as the upstream plane for calculation of the blunt fin flow. The surface boundary conditions were the standard no-slip, adiabatic wall conditions with zero normal pressure gradient. Zero gradient conditions were applied on the downstream and normal boundaries, to ensure the flow remained unperturbed along the fin and at large distances from the intersection of the surfaces.

SECTION III

RESULTS

1. FLAT PLATE OIL STREAKS

Simulation of oil streaks on the flat plate surface is one method of evaluating the upstream and spanwise effects of the presence of the blunt fin in the flow field. Figure 5

presents the computed streak patterns from the present study for the case of the vertical fin. The reference lines on the flat plate are 1/2 diameter apart. The similarity between these results and those shown in Figure 2 is clear. The primary convergence line for the present calculation is slightly more than two diameters upstream of the fin leading edge, and does not recede downstream as quickly as the computed convergence line shown in Figure 2. In this respect the current calculation more closely resembles the experimental results, shown as the dashed line in Figure 2. The extent of spanwise disturbance can be judged from the location of the convergence line as it recedes downstream and outward past the fin. At the fin leading edge, the spanwise location of the limiting streamline is 3.8 diameters, increasing to 5.2 and then 6.3 diameters at stations two and four diameters downstream of the leading edge, respectively. Figure 6 shows similar views of the oil patterns computed for cases of fin sweepback of 30°, 45°, 60°, and 68°. The upstream location of the convergence line approaches the fin steadily as the sweepback increases, although there is a distinct accumulation line upstream of the fin even at 60°.

At the sweepback angle of 68°, however, no convergence line can be found upstream of the leading edge. This corresponds to the bifurcation point: a new phase portrait of the surface shear-stress vector has emerged. There is a simultaneous

change in the external flow pattern associated with the phase portrait. The horseshoe vortex, which previously was the mechanism for diverting oncoming fluid around the fin, no longer exists. What may appear to be a convergence line spreading spanwise from the leading edge of the fin is actually a cluster of parallel streamlines which are forced into close proximity due to the deflection of the flow originating upstream of the fin. The region between these compressed streamlines and the blunt fin is occupied by fluid which passes over the top of the fin before sweeping down. By comparing the location of the computed oil patterns with those for the previous sweepback angles, one can see that the extent of the disturbed flow is very small for this case. This decreasing spanwise propagation of disturbance is in a consistent trend with the assertion that increasing fin sweepback indicates weakening of the horseshoe vortex. The effect of the sweepback on the spanwise location of the oil accumulation line is summarized in Figure 7, which plots the convergence line location versus sweep angle for the range of zero to sixty degree sweep.

2. FLAT PLATE PRESSURE DISTRIBUTION

Although the location of the oil convergence line gives an indication of where the flow leaves the surface to roll up into vortical structures, it does not specifically define the

extent of fin influence on the flow field. One other parameter which can help define this influence is the distribution of pressure on the flat plate. The surface pressure distribution in the plane of symmetry for the vertical fin is presented in Figure 8. This pressure distribution reveals the strong influence exerted by the embedded horseshoe vortical structure. Twin pressure peaks are partitioned by a trough which is induced by the presence of a strong primary vortex system attached to the surface. The present calculation produces good agreement with previous experiments and calculations. The dip in pressure near the leading edge of the blunt fin is similar to the dip observed in the calculations of Reference 7 when a refined grid was used.

The particular behavior of the surface pressure at the plane of symmetry persists beyond the blunt leading edge of the fin. The twin peaks characterizing the distribution are diminished by the rapid expansion around the leading edge and by the dissipation of the horseshoe vortex as the flow moves downstream. This process can be observed in the contours of pressure on the flat plate, shown in Figure 9 for both experimental and computational results. Examination of Figures 9a and b reveal an excellent agreement between experiment and computation for the vertical fin. The initial limit of disturbance is approximately 2.7 diameters upstream of the fin, receding to less than one diameter upstream of the fin at a

spanwise station of four diameters. The first peak pressure upstream of the fin leading edge is in the vicinity of 1.3 diameters upstream, although the peak is somewhat smeared in the calculation. The location of the pressure trough downstream of the first peak corresponds to the experimentally determined location. The propagation of the trough and the expansion around the fin also compare very well with experimental measurements. In Figure 9c, $\Lambda=30°$, one can observe that the initial pressure disturbance has receded to one diameter upstream of the fin leading edge. The first peak pressure retains the same magnitude as that for the vertical fin, but is located much closer to the fin. The pressure trough also doesn't change significantly in magnitude, although it does change in location. The final peak pressure on the fin is lower than the counterpart on the vertical fin. The spanwise propagation of flow disturbance is also lessened significantly, as the pressure disturbance does not reach a spanwise station of four diameters until more than two diameters downstream of the fin leading edge. For cases of sweepback of 45, 60, and 68 degrees, the first peak pressure upstream of the fin leading edge remains remarkably constant. The pressure trough between the first and final pressure peaks becomes less pronounced with greater sweepback, however, while the final peak pressure decreases in magnitude. The result is that at a sweepback between 60 and 68 degrees, the pressure trough disappears entirely and there is only one pressure peak.

This coincides with the bifurcation of the surface shear portrait and the disappearance of the horseshoe vortex upstream of the fin. The spanwise disturbance also continuously decreases, until at 60 degrees, the disturbance reaches four spanwise diameters at a downstream station of five diameters.

3. VORTICAL STRUCTURES

The primary mechanism associated with diverting fluid past the blunt fin is a horseshoe vortex which forms upstream of the fin. The structure of this vortex for the vertical fin in the plane of symmetry can be seen by the particle traces of Figure 10. In this and following figures, the reference coordinate lines on the flat plate are 1/2 diameter apart. The center of the vortex is located slightly more than 1/2 diameter upstream. This corresponds to the location of the pressure trough upstream of the blunt fin in Figure 9b. Figure 11 shows the overhead view of the trajectory of particles swept into this vortex. Again comparison with Figure 9b shows a strong correlation between the vortex trajectory and the pressure trough present in the flow field. For example, at a distance of two diameters downstream of the fin leading edge, the computed vortex particle traces pass a location at three diameters outboard of the center line. This coincides with the experimental and computed location of the pressure trough. Figures 12-14 show further evidence to substantiate this

correspondence. Note that in these figures, the blunt fin is not shown for clarity. Figure 12 shows the vortex trajectory for Λ=30°. At a station 1/2 diameter downstream of the fin leading edge, the center of the vortex is located at a distance of one diameter from the center line. This coincides closely with the location of the pressure defect as plotted in Figure 9c. The center of the vortex in the symmetry plane is located at roughly .2 diameters of the leading edge of the fin, which again closely correlates to the location of the pressure trough in Figure 9c. From Figure 13, Λ=45°, one can see the vortex situated a very small distance upstream of the fin, and at one diameter downstream, the vortex is located slightly more than one diameter spanwise from the center line. These results again agree with the computed location of the pressure trough (Fig. 9d). As the sweepback angle becomes greater, the vortex gradually decreases in size, which also corresponds to the weakening of the pressure trough shown with increasing sweepback angle. Figure 14 shows the continuation of this trend. Here, the vortex forms directly above the fin leading edge and is still located within one spanwise diameter of the blunt fin when it is one diameter downstream of the leading edge. By this time the dimension of the vortex is smaller than 1/20th the boundary layer thickness in diameter and shows little effect on the mean flow. This observation can be confirmed by the pressure contour plot Fig. 9d, which shows only a slight wiggle in the contours near the intersection of

the fin and the plate to indicate the existence of the pressure drop. Figure 15 is an elevated view of the flow field very near the fin-flat plate juncture for $\Lambda=68°$. It is apparent, as stated before, that no vortex formation is present. Upstream fluid particles approaching the fin simply divert to the side of the fin without being entrained by a vortical structure, or continue up the fin before passing down its side.

SECTION IV

CONCLUSION

The flow past a blunt fin at Mach 2.95 was successfully calculated for several fin sweepback angles. Numerical results show that the flow field topological structure undergoes a bifurcation at sufficiently high angles of sweepback. Sweepback of the fin reduces the upstream influence of the flow field and simultaneously weakens the horseshoe vortex upstream of the fin. Spanwise influence is thereby decreased. For the simulated conditions, the horseshoe vortex ceased to exist between 60 and 68° sweep.

REFERENCES

1. Korkegi, R. H., "Survey of Viscous Interactions Associated with High Mach Number Flight," AIAA Journal, Vol. 9, May 1971, pp. 771-784.

2. Price, A. E. and Stallings, R. L., "Investigation of Turbulent Separated Flows in the Vicinity of Fin Type Protuberances at Supersonic Mach Number," NASA TN D-3804, February, 1967.

3. Burbank, P. B., Newlander, R. A., and Collins, I. K., "Heat-Transfer and Pressure Measurements on a Flat-Plate Surface and Heat-Transfer Measurements on Attached Protuberances in a Supersonic Turbulent Boundary Layer at Mach Numbers of 2.65, 3.51, and 4.44," NASA TN D-1372, December, 1962.

4. Dolling, D. S. and Bogdonoff, S. M., "Blunt Fin-Induced Shock Wave/Turbulent Boundary Layer Interaction," AIAA Journal, Vol. 20, December 1982, pp 1674-1680.

5. Dolling, D. S., Cosad, C. C., and Bogdonoff, S. M., "An Examination of Blunt Fin-Induced Shock Wave Turbulent Boundary Layer Interactions," AIAA Paper 79-0068, January, 1979.

6. Hung, C.-M., and Kordulla, W., "A Time-Split Finite-Volume Algorithm for Three-Dimensional Flowfield Simulation," AIAA Journal, Vol. 22, November 1984, pp. 1564-1572.

7. Hung, C.-M., and Buning, P. G., "Simulation of Blunt-Fin-Induced Shock-Wave and Turbulent Boundary-Layer Interaction," Journal of Fluid Mechanics, Vol. 154, 1985, pp. 163-185.

8. Shang, J. S. and Scherr, S. J., "Navier-Stokes Solution for a Complete Re-Entry Configuration," Journal of Aircraft, Vol. 23, December 1986, pp. 881-888.

9. Tobak, M. and Peake, D. J., "Topology of Three-Dimensional Separated Flows," Annual Review of Fluid Mechanics, Vol. 14, 1982, pp. 61-85.

10. MacCormack, R., W., "The Effect of Viscosity in Hypervelocity Impact Cratering," AIAA Paper 69-354, January 1969.

11. Shang, J. S., Hankey, W. L., and Petty, J. S., "Three-Dimensional Supersonic Interacting Turbulent Flow along a Corner," AIAA Journal, Vol. 17, July 1979, pp 706-713.

12. Hung, C. M., and MacCormack, R. W., "Numerical Solution of Three-Dimensional Shock Wave and Turbulent Boundary-Layer Interaction," AIAA Journal, Vol. 16, October 1978, pp 1090-1096.

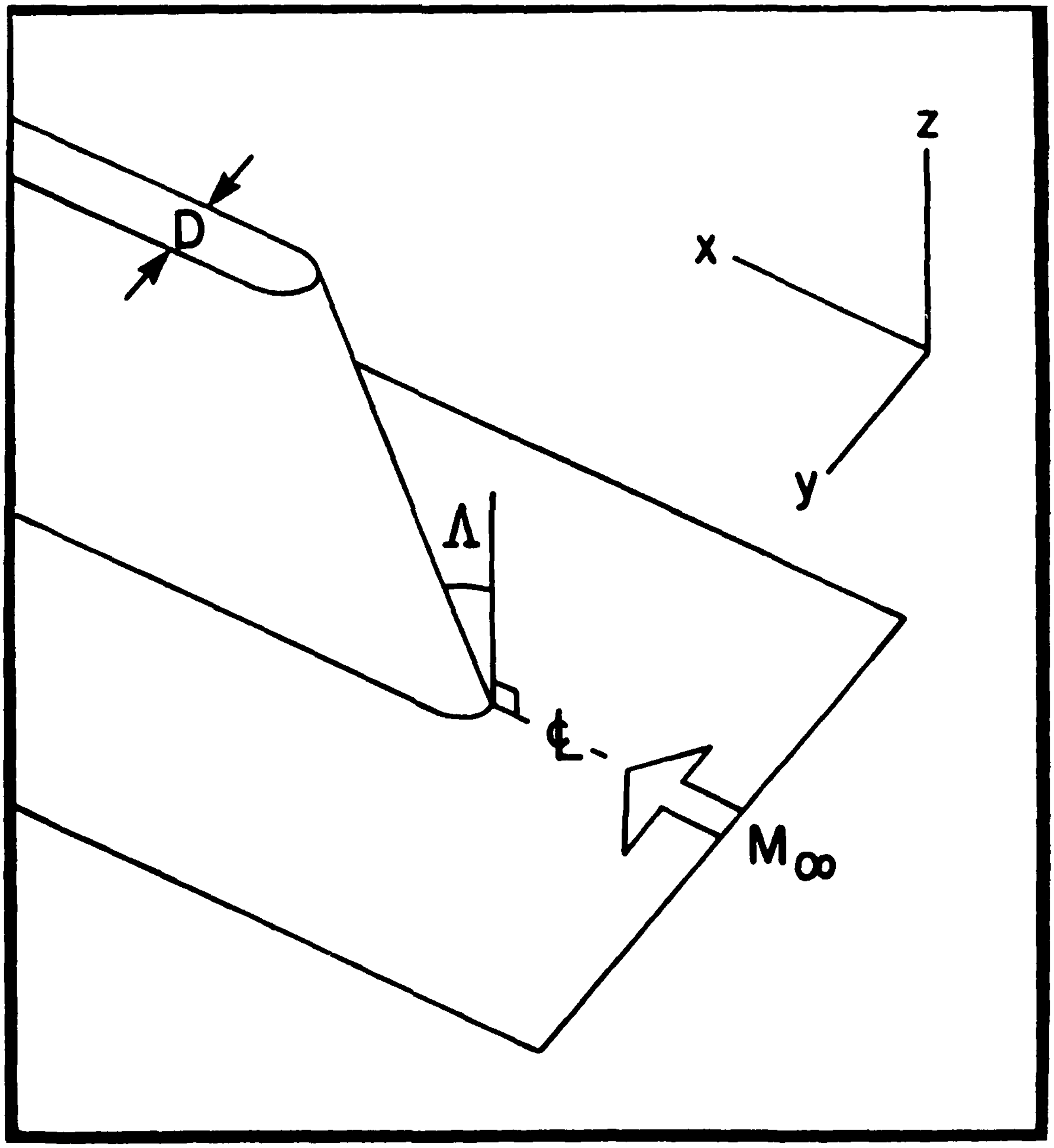

Figure 1: The Baseline case for the Blunt Fin Control Surface is the Blunt Fin on a Flat Plate at Zero Angle of Attack to the Freestream

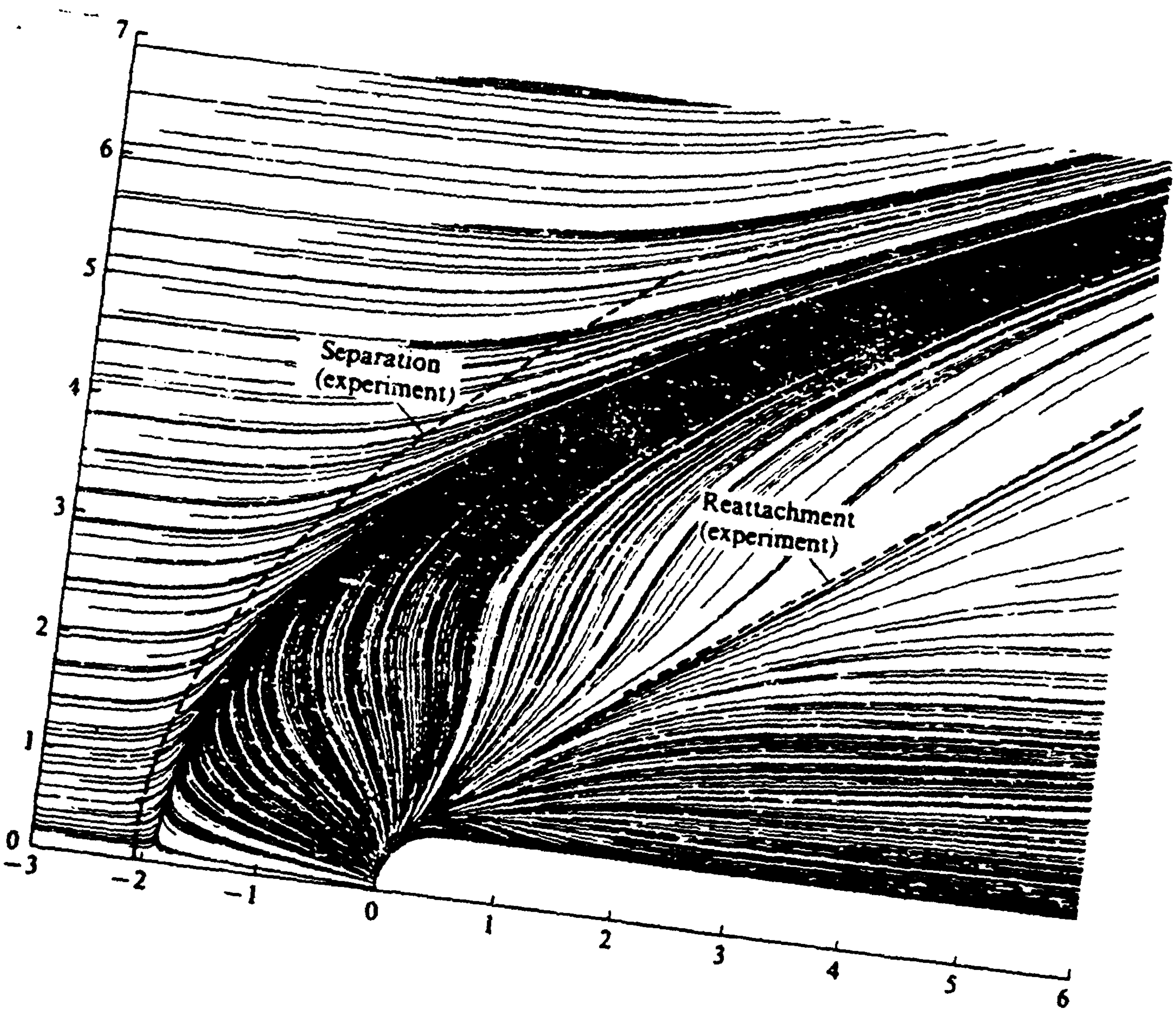

Figure 2: The Flow Past a Vertical Blunt Fin is Characterized By a Surface Oil Pattern on the Flat Plate That Includes a Convergence line and a divergence line

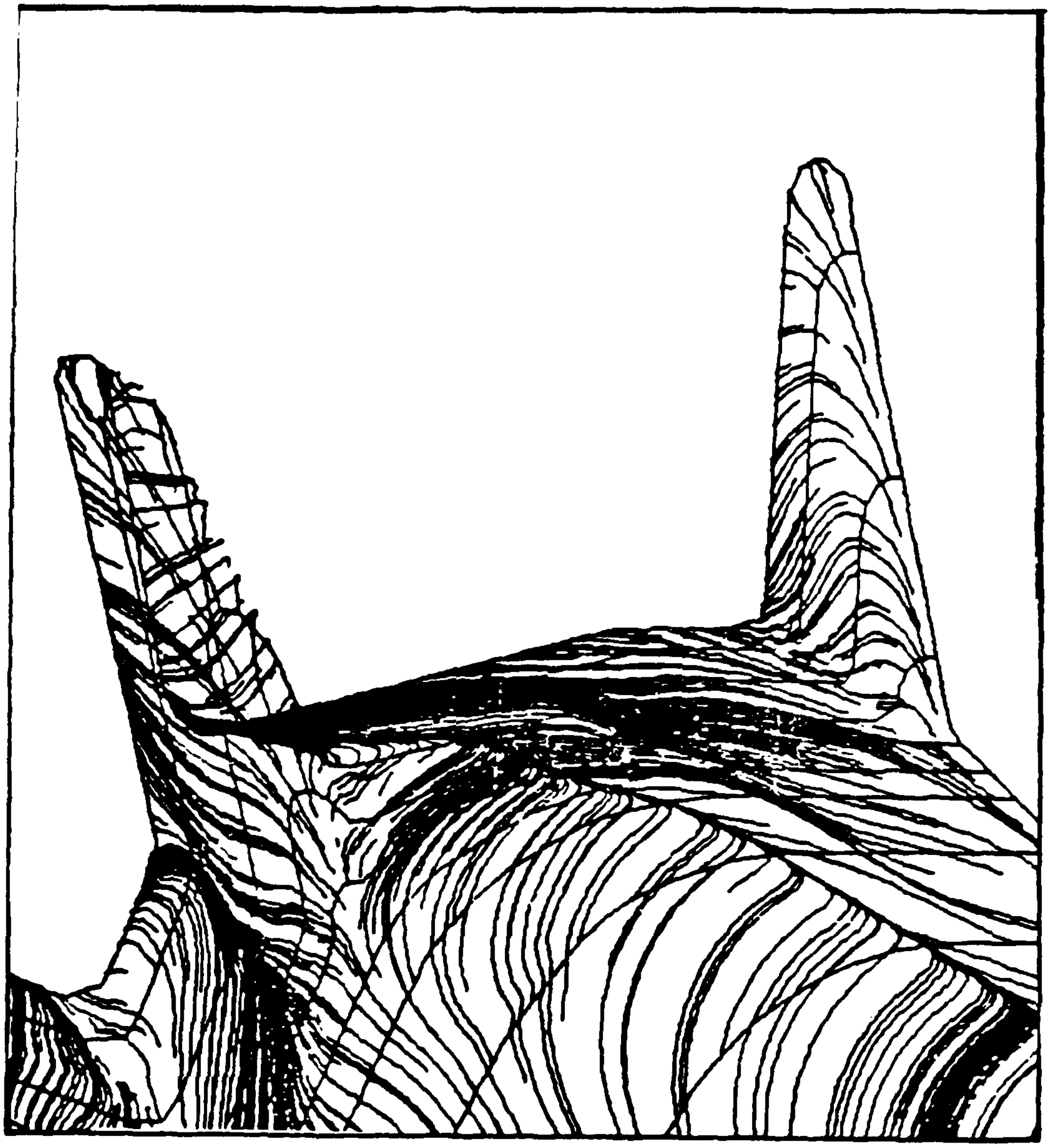

Figure 3: Surface Shear Pattern Near a Highly Swept Fin on a Complex Body

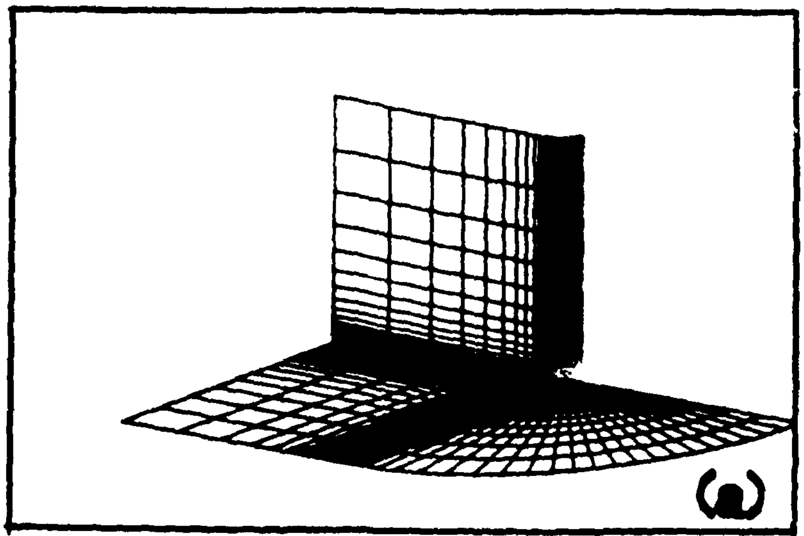

Figure 4a: Elevated View of the Grid Used to Compute the Flow Past The Vertical Fin

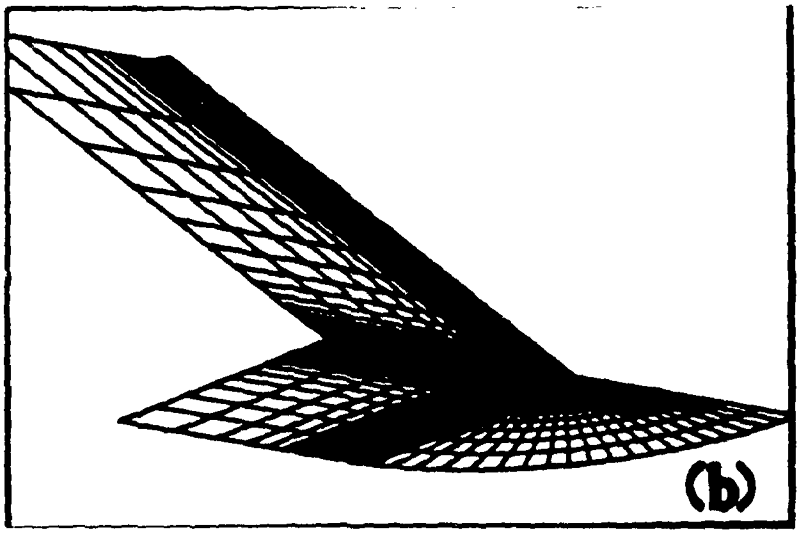

Figure 4b: Elevated View of the Grid for the 60° Swept Fin

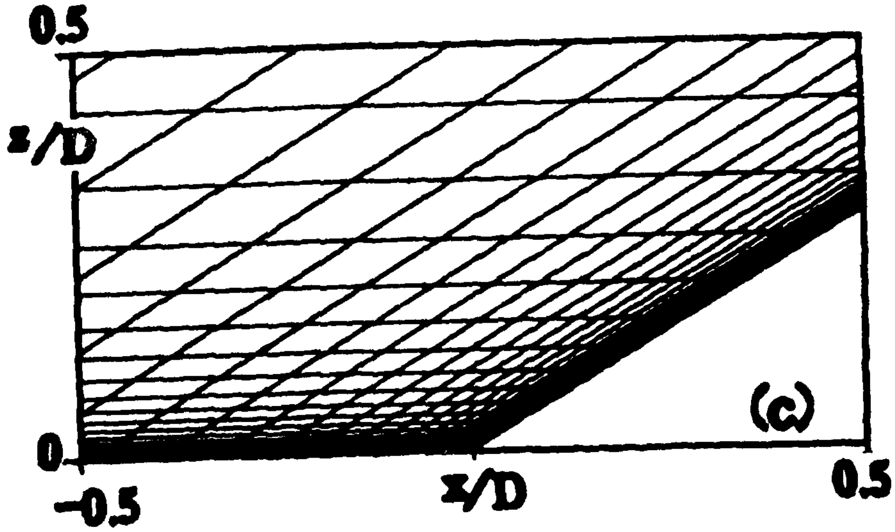

Figure 4c: A Closeup of the Grid Cells Near the Fin-Flat Plate Junction on the Plane of Symmetry

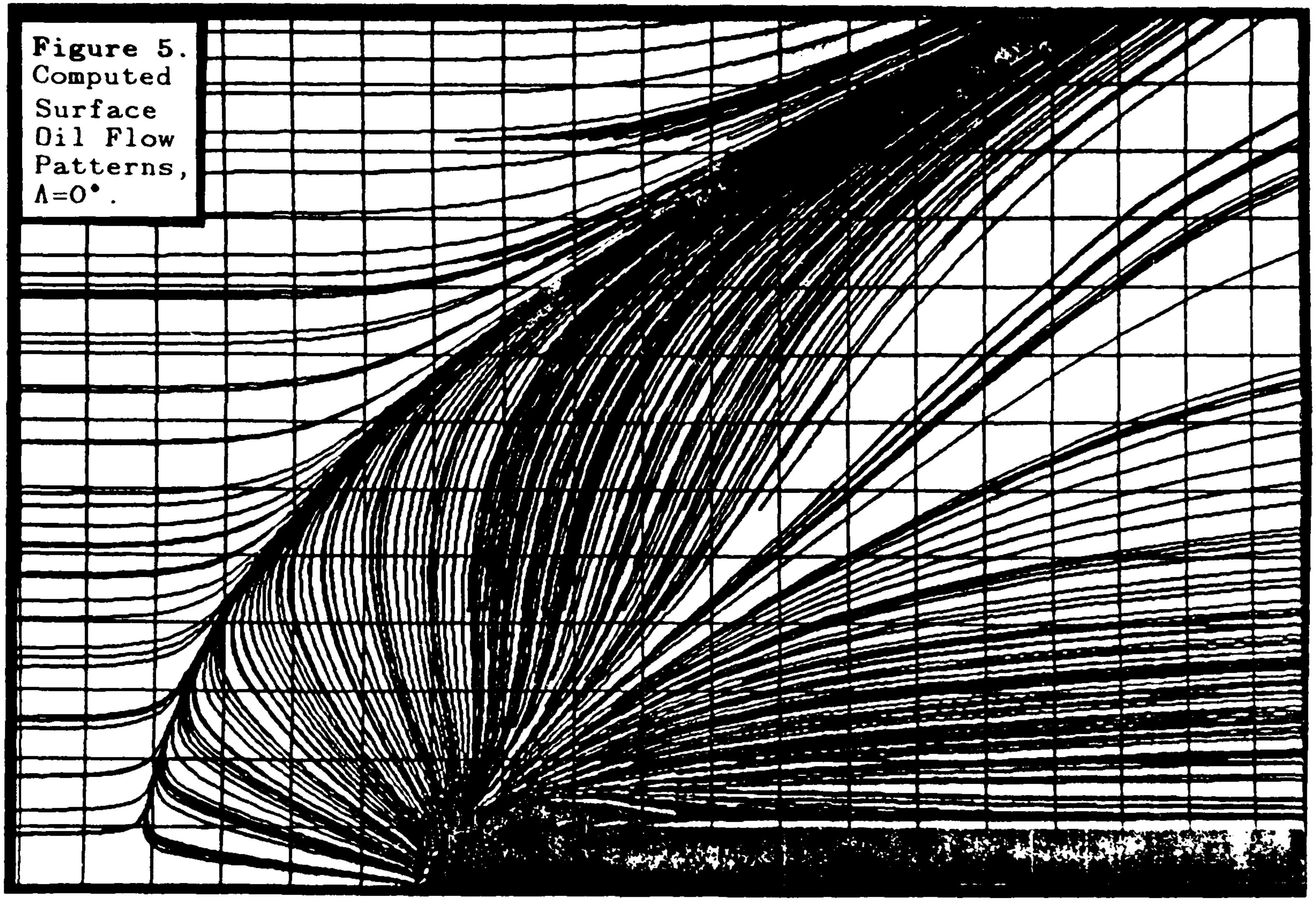

Figure 5: The Computed Streak Patterns From the Present Study for the Case of The Vertical Fin

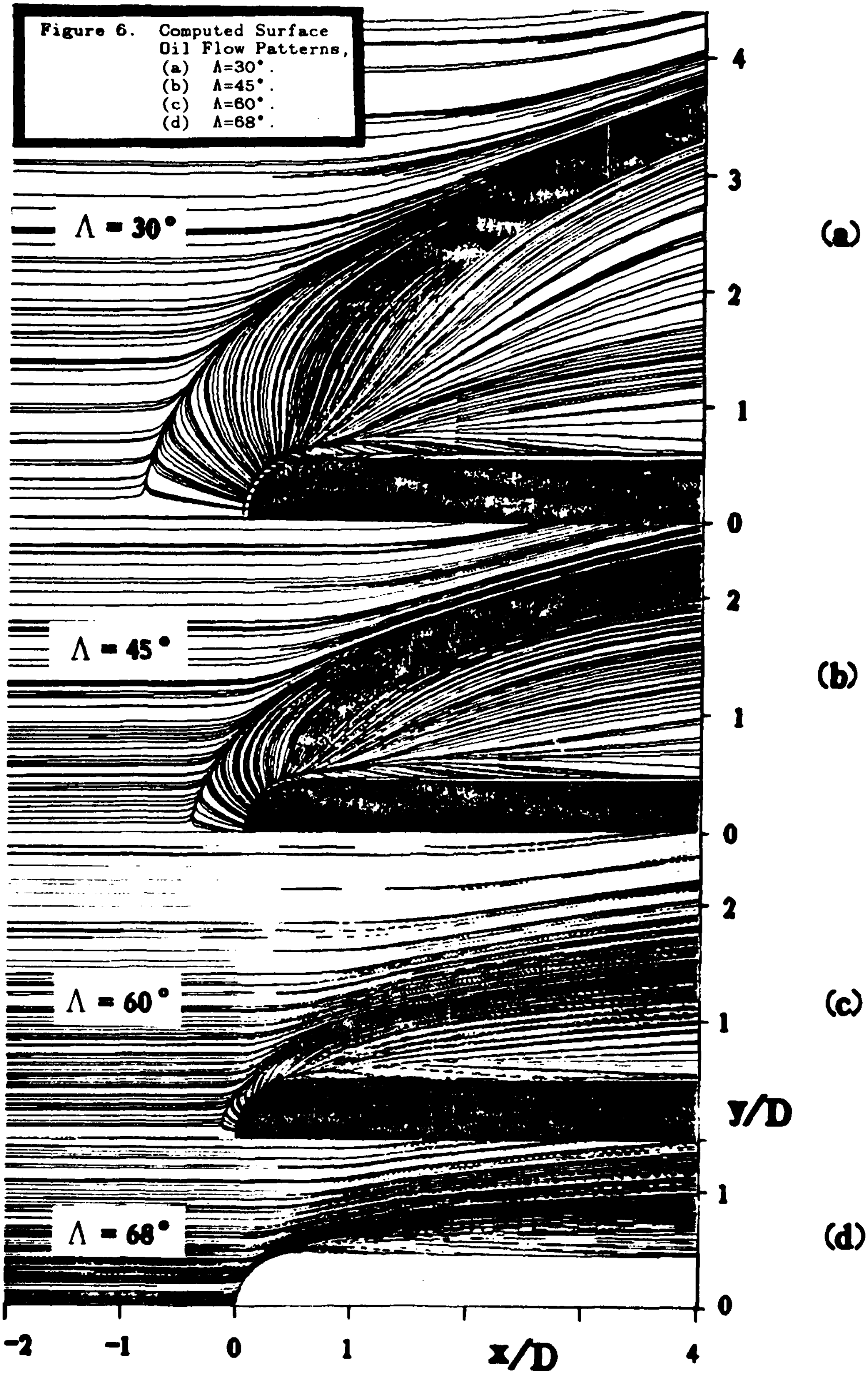

Figure 6: The Oil Patterns for Cases of Fin Sweepback of 30°, 45°, 60°, and 68°

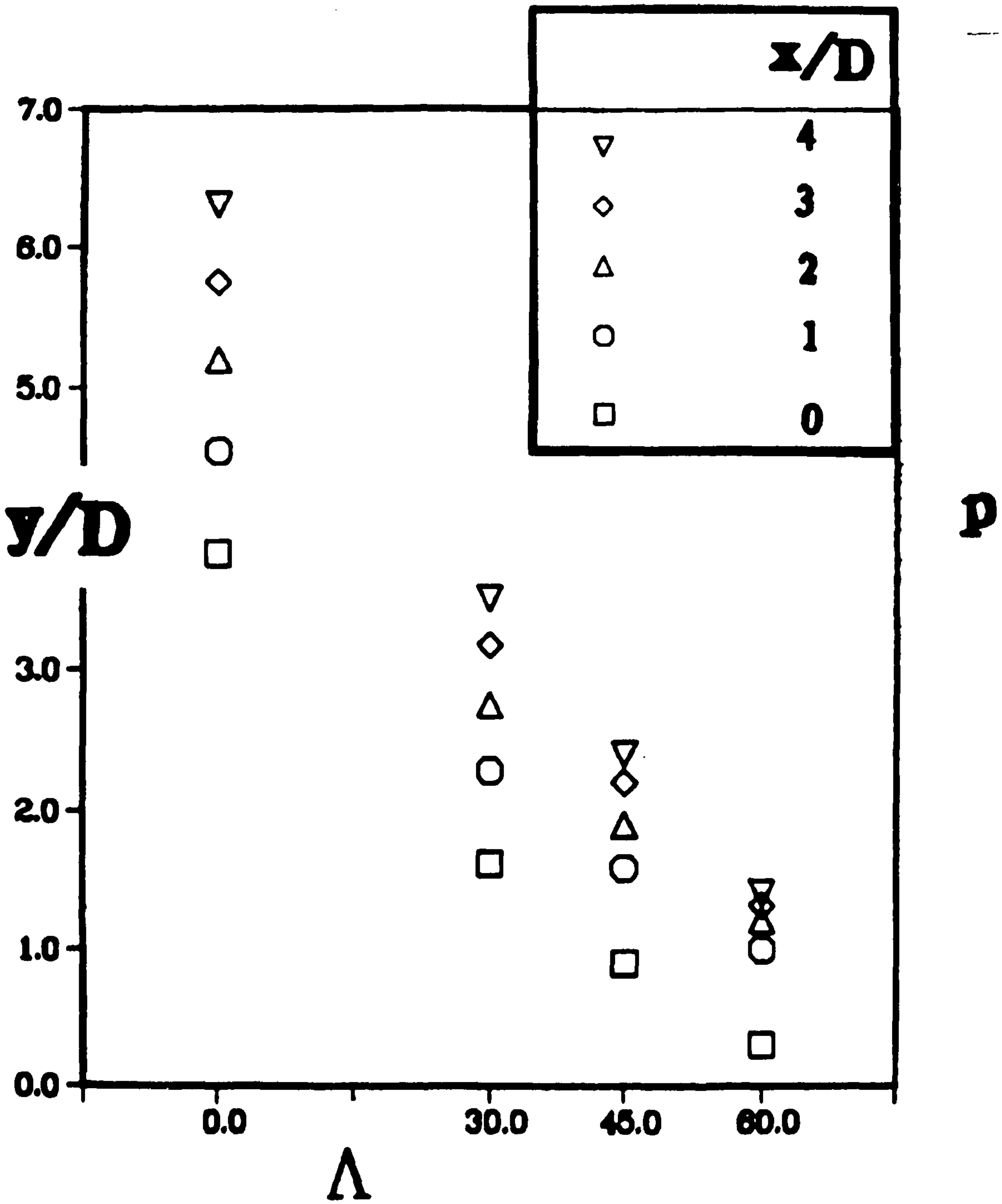

Figure 7: Plots the Convergence Line Location Versus Sweep Angle for the Range of Zero to Sixty Degree Sweep

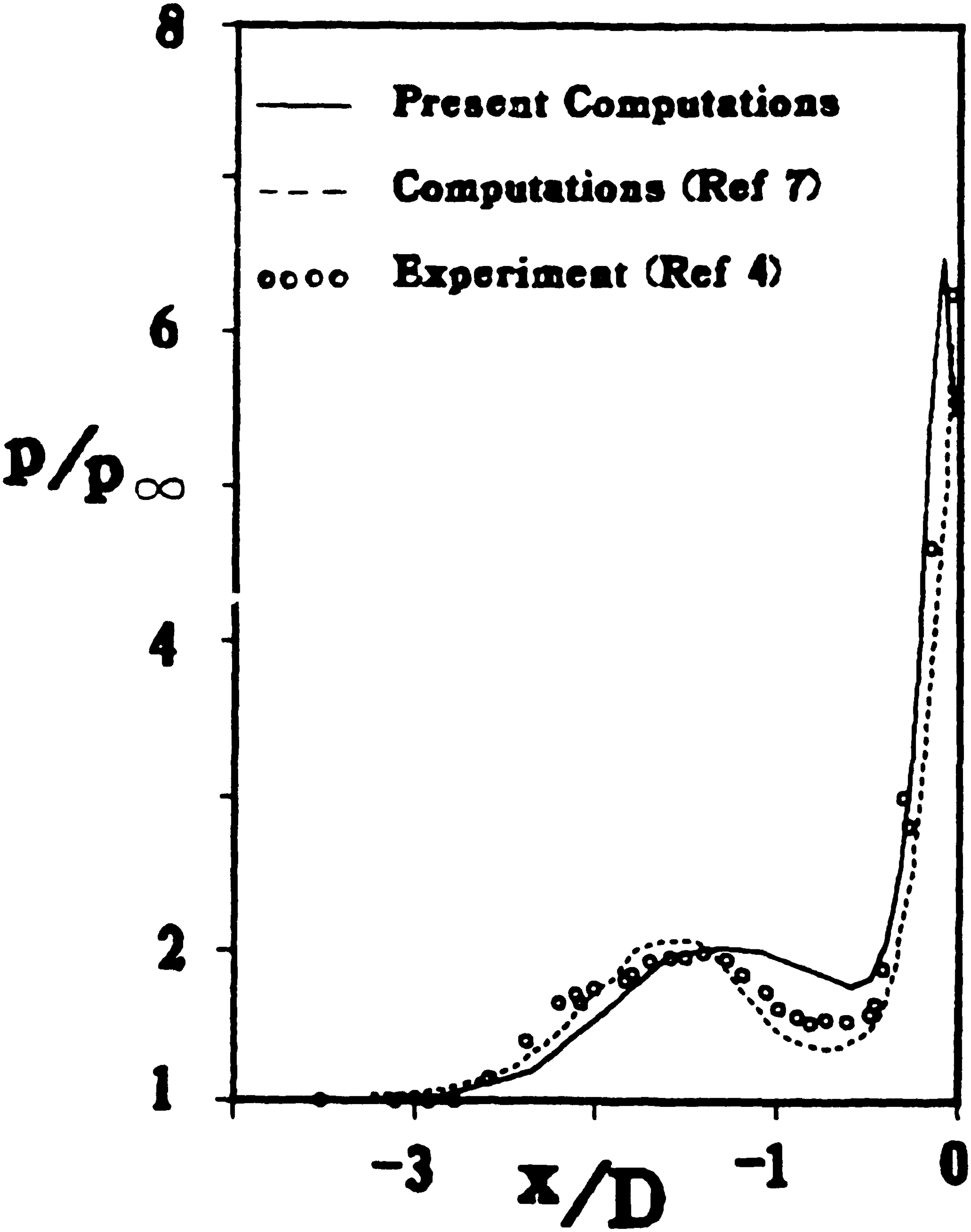

Figure 8: The Surface Pressure Distribution in the Plane of Symmetry for the Vertical Fin

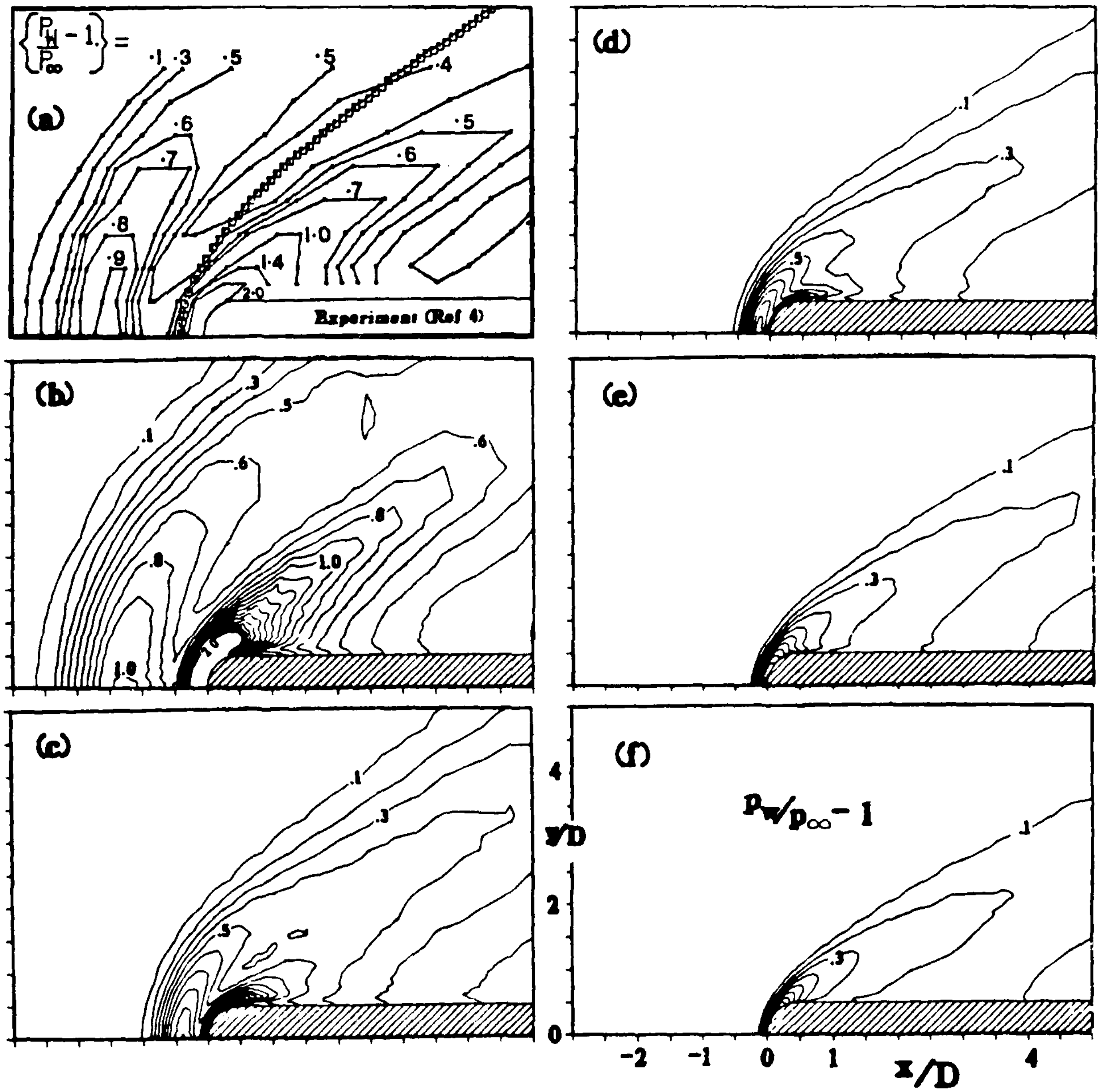

Figure 9: The Contours of Pressure on the Flat Plate

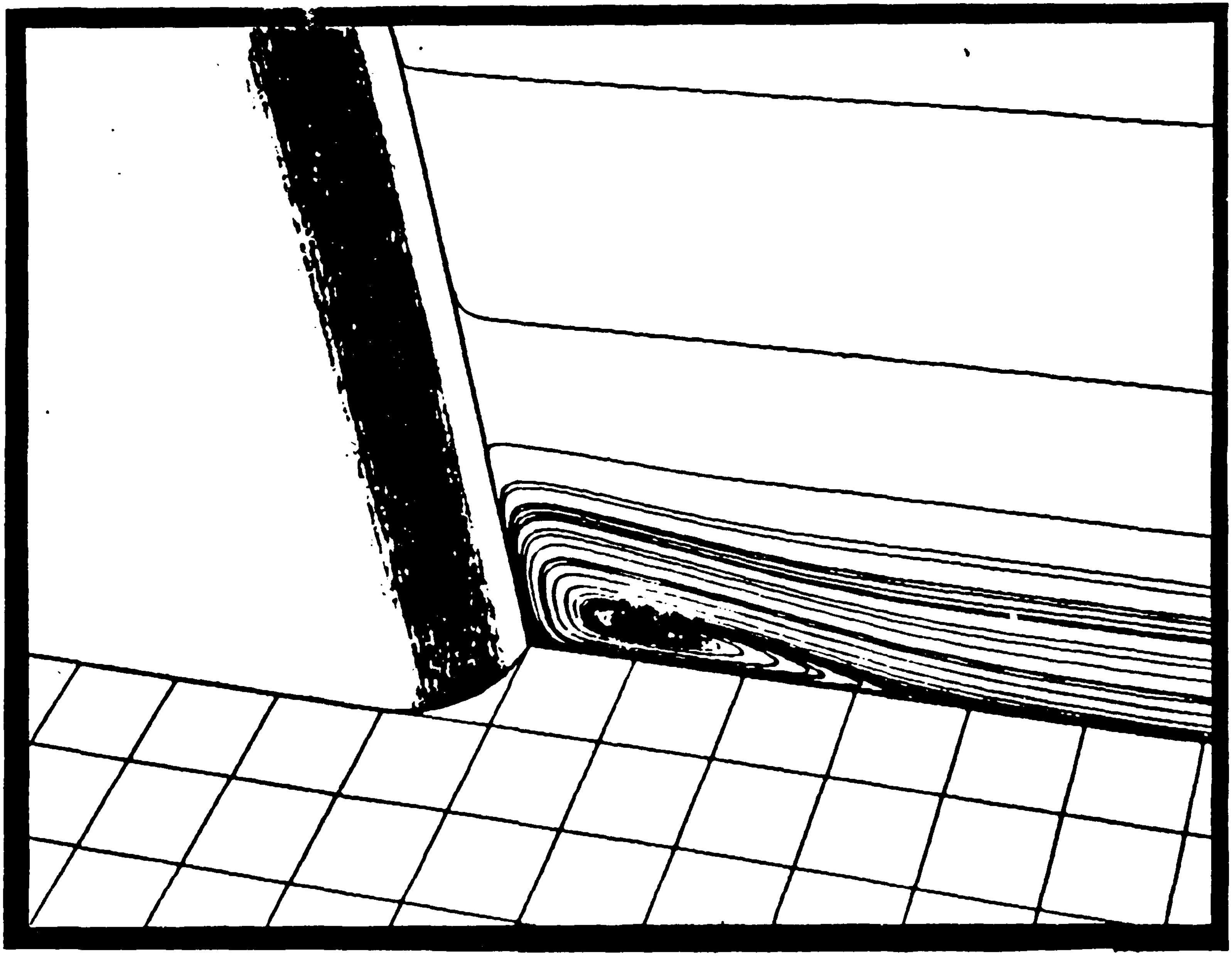

Figure 10: Diverting Fluid Past the Blunt Fin is a Horseshoe Vortex Which Forms Upstream of the Fin

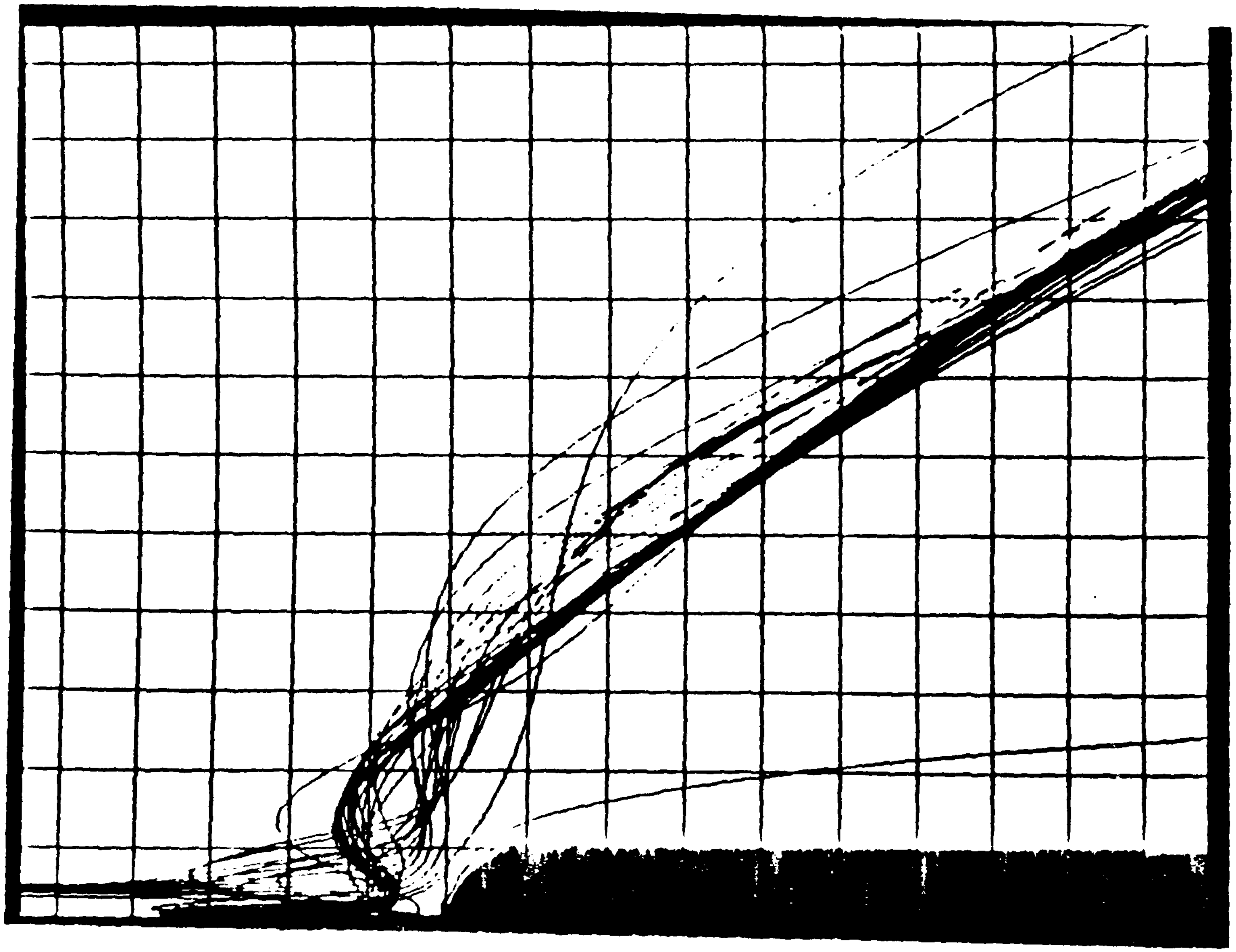

Figure 11: Spanwise Trajectory of Vortex, A ~ 0°

Figure 12: Vortex Trajectory for A = 30°

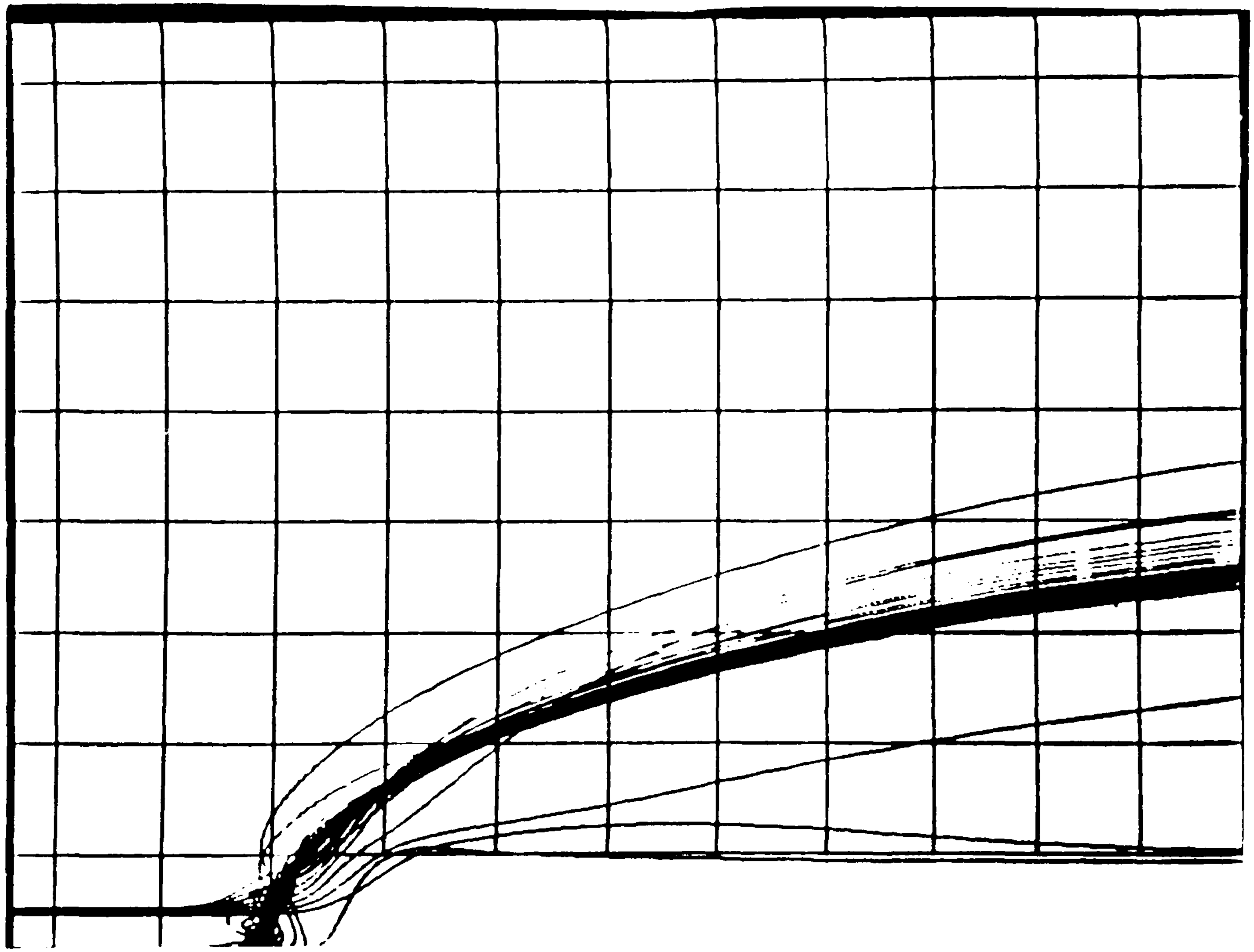

Figure 13: A = 45° the Vortex Situated a Very Small Distance Upstream of the Fin, and One Diameter Downstream

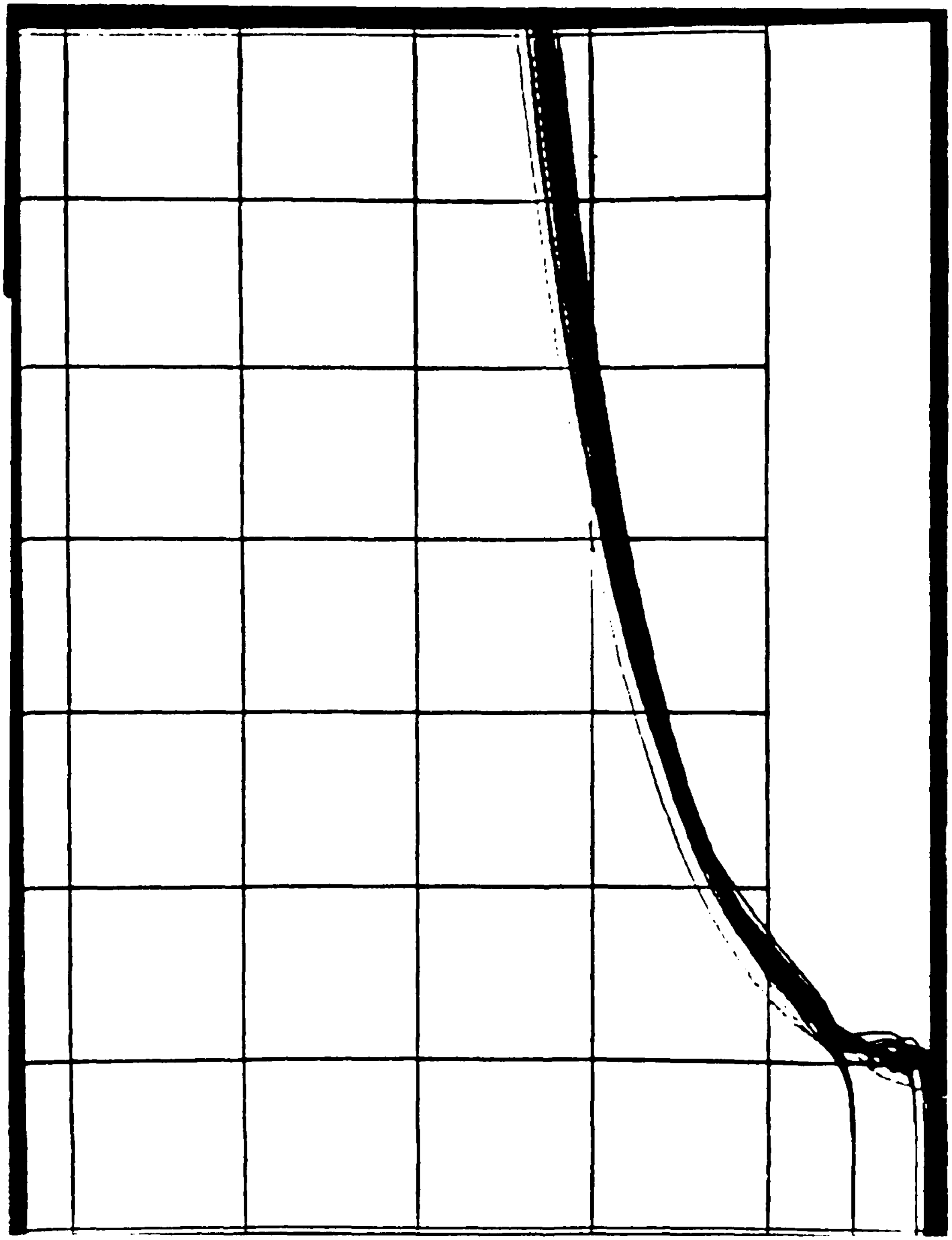

Figure 14: Shows the Continuation of the Trend

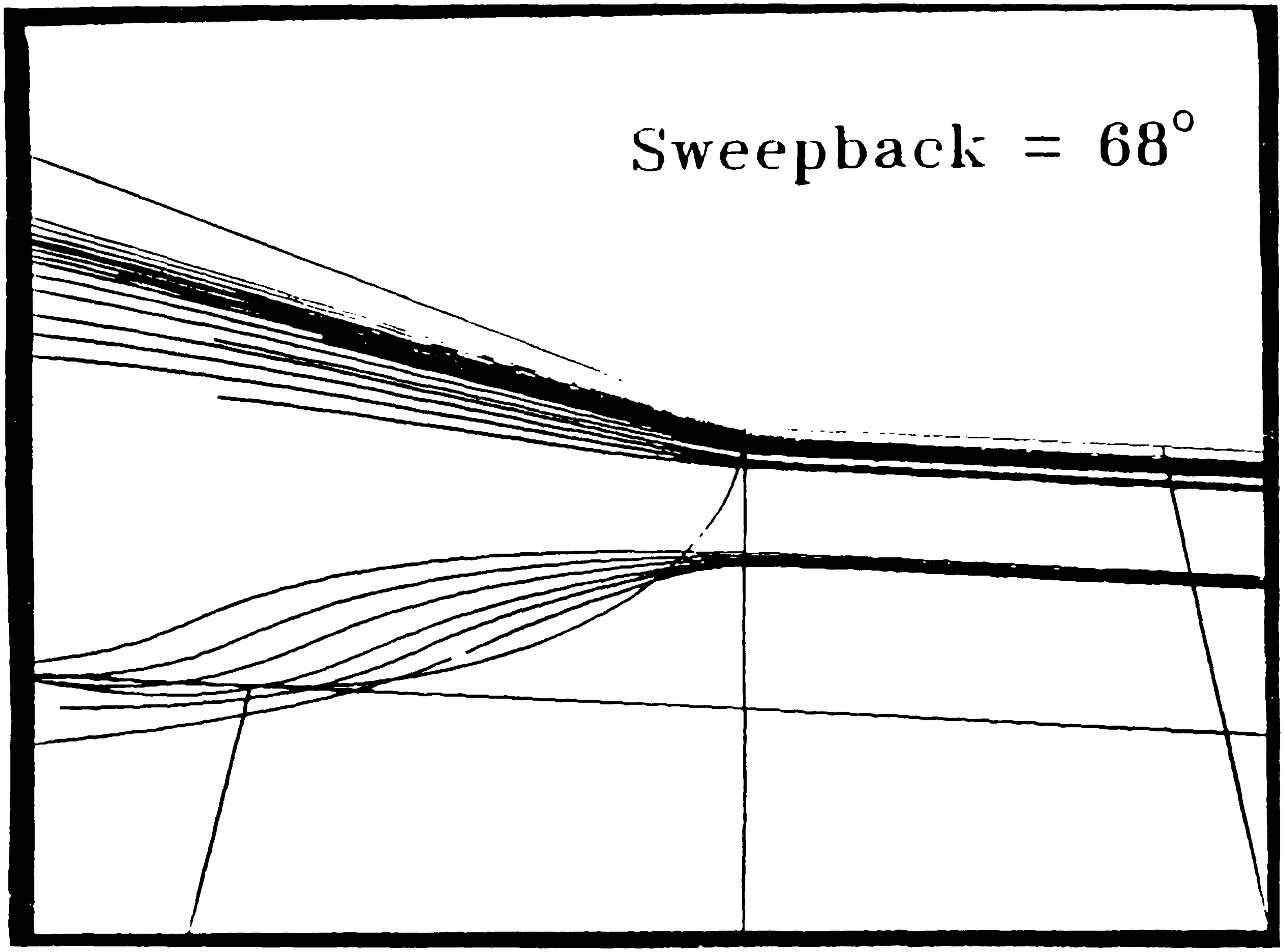

Figure 15: Elevated View of the Flowfield Very Near the Fin-Flat Plate Juncture for A = 68°

U.S. GOVERNMENT PRINTING OFFICE 1988 - 648-001/80309